Received: 21 November 2023 | Revised: 9 January 2024 | Accepted: 18 January 2024 | Published online: 22 January 2024

RESEARCH ARTICLE

Archives of Advanced Engineering Science
2025, Vol. 3(2) 111–123
DOI: 10.47852/bonviewAAES42022110

BON VIEW PUBLISHING

Analysis of Grid-Tied Solar Photovoltaic Energy Generation Under Uncertain Atmospheric Conditions Using Adaptive Neuro-Fuzzy Control System

Ja'afar Sulaiman Zangina[1,*], Muhammad Aliyu Suleiman[2] and Abdulla Ahmed[3]

[1]*Food and Industrial Biotechnology, National Biotechnology Development Agency, Nigeria*

[2]*Software Engineering Department, Nile University of Nigeria, Nigeria*

[3]*Department of Electrical and Electronics Engineering, University of Nyala, Sudan*

Abstract: The grid-tied photovoltaic (PV) power system has remained the most practical and sustainable configuration among renewable energy generation systems. Although uncertainties persist in solar irradiance and temperature, the grid-tied system faces transient instability issues during maximum power point tracking, adversely affecting power quality and resulting in substantial costs. To overcome this issue, we proposed analyzing the grid-tied system under uncertain atmospheric conditions based on an adaptive neuro-fuzzy control system (ANCS). This control scheme incorporates a hybrid learning algorithm and undergoes evaluation across various operating conditions. The obtained results demonstrate the effectiveness of the learning algorithm in maintaining a fast convergence speed. Consequently, this capability ensures the consistent preservation of sufficient power quality in the power system without any discernible transient impact. Furthermore, the investigation reveals the significant impact of solar radiation and temperature on the performance of the solar grid-tied PV system. Specifically, temperature alone contributes to over 15% power reduction when reaching 45 °C. As the temperature decreases to 5 °C at 1000 W/m^2 irradiance, the ANCS influences an increase in the system's power generation from 100.72 kW at 25 °C to 103.01 kW.

Keywords: adaptive neuro-fuzzy, grid-tied photovoltaic system, hybrid learning algorithm, power quality, zero transients

1. Introduction

There is a growing use of solar photovoltaic (PV) as a renewable energy source because of the number of advantages it provides. These include simplicity, ease of installation, negligible maintenance, noiseless operation, and above all, zero carbon emission. The progress recorded in solar PV technology has driven the installation cost of the solar power system [1–7]. These increased the number of solar PV integration in the power network and eventually introduced new challenges. The challenge includes poor power quality, like harmonic distortion, unstable voltage supply, and frequency variation. Several efforts from the research community have yielded significant results in terms of the solar PV system connection to a grid. Yet more is required to tackle emerging challenges like persistent failure, associated operational challenges, and increased demand for reactive power [8–14]. Grid-tied PV systems emerged from a long-time research effort to replace PV stand-alone systems. The grid-connected PV system has turn to a popular design of consistent electric source. The connected PV system is designed and operates a grid-interactive pulse width modulation, utilizing voltage source inverter (VSI) to achieve high efficiency [15, 16]. VSI connection requires optimal power extraction, independent control of active/reactive power supplied to the electrical grid, excellent transient response and grid synchronization, etc. However, in the case of a low-power PV array, a boost converter is employed to perform maximum power point tracking (MPPT) and raise the voltage of the PV source to align with the voltage of the DC link [17]. These techniques are usually employed to maintain a stable power supply from the PV system to the distributed generation network.

The current work contribution includes the adaptive control MPPT based on the neuro-fuzzy system application on a three-phase grid-tied PV system coupled with a feeder network. In addition, the study contributes by conducting a stability analysis of the integrated PV system in the presence of various atmospheric disturbances. However, the motivation behind the proposed adaptive neuro-fuzzy control system (ANCS) for grid-tied PV power systems lies in addressing the challenges posed by uncertainties in solar irradiance and temperature.

1.1. Problem

The distributed energy resources integration into the power network has raised the vulnerability of the power supply quality to

***Corresponding author:** Ja'afar Sulaiman Zangina, Food and Industrial Biotechnology, National Biotechnology Development Agency, Nigeria. Email: jaafzangs@nabda.gov.ng

poor power quality in the power system network. Therefore, fluctuating supply from one PV system can be costly not only to the network of electrical power systems but also to the power end-user [18]. This challenge required a robust control strategy capable of adequately tuning the state parameters to achieve a sustainable seamless power supply. In recent years, more research has concentrated on MPPT technology while considering atmospheric conditions' influence [19]. To effectively investigate the impact of the MPPT techniques, PV generation under uncertain atmospheric conditions needed to be studied.

1.2. Related work

Several reported MPPT techniques have a promising performance, including the perturb and observe (P&O) method alongside incremental conductance [20–22]. These techniques have a complex implementation procedure and are a bit weak in handling solar irradiation uncertainty, and achieving a global maximum power point became difficult [23, 24]. Also, these tactics are identified with slow response time to a maximum power point due to their high oscillatory sensitivity and poor convergence rate. However, several efforts from different research groups have contributed to the ameliorating deficiency of the techniques. These efforts are in the design process and operation strategy, which includes algorithm modification, variable step size, and new framework development [24–31]. The achieved progress includes enhanced convergence rate and tracking of the PV scheme during varying weather conditions compared with the traditional techniques.

Despite the effort made by improving the conventional techniques, more MPPT-enhanced strategies are needed to balance the PV system's performance and its global capability in maximizing power output. However, some methods proposed based on the soft computing paradigm to address a complex system's dynamic behavior and PV power flows. A technique based on the grey wolf algorithm, artificial intelligence, and evolutionary algorithm approach deployed was to tackle the nonlinear features of the PV system [32–38]. Although soft computing-based techniques have a complex computational process, they have better performance. Adequate tracking and convergence speed obtained on a grid linked PV framework with an extremum seeking algorithm [39–42]. This control strategy employed algorithms to estimate the gradient of the generated power iteratively. However, system operation stability with global MPPT while maintaining a fast convergence rate can be difficult. Hybrid techniques for power point tracking were also employed using differential evolution and particle swarm optimization algorithm to improve MPPT. These methods exhibit a promising performance while dealing with irradiance uncertainty during PV energy generation [43]. Despite the performance of the classical tracking method for peak power such as incremental conductance, P&O with an enhanced algorithm, soft computing techniques remain robust. Although the method was associated with a computational burden, it deals with rapid atmospheric variation and partial shading.

1.3. Our approach

The current study focuses on applying adaptive control in MPPT based on a neuro-fuzzy control system to maintain grid-tied PV system stability under the uncertain disturbance of atmospheric conditions. Fast variation of atmospheric conditions is an important issue in the PV generation framework, as the occurrence produces harmonic distortion in the inverter output connected to the power network. The projected control scheme will keep track of the global maximum power point to generate an appropriate control signal for the optimum operation of the inverter through the converter. This control strategy can guarantee grid power quality with zero transient current and voltage during atmospheric uncertainty in the PV system. These are achievable by the control system because of the soft switching and seamless operations capability.

1.4. Novelty

Our work is novel because while some previous work has used type 1 or type 2 fuzzy logic on a single-phase grid-tied network, they did not explore adaptive hybrid neuro-fuzzy logic on three phases grid-tied PV system to control its stability under the uncertain disturbance of atmospheric conditions. In summary, the current work has contributed the following to the investigation of the impact of the MPPT approaches and PV generation under uncertain atmospheric conditions: (1) the adaptation of the adaptive control MPPT built on the neuro-fuzzy scheme for three phases grid-tied PV system coupled with a feeder network, (2) implementation of a stability analysis of the integrated PV system under the influence of different atmospheric disturbances, (3) hypothesize that hybrid learning algorithm consolidation within the control architecture enables zero transients in the size of the current power infrastructure network, and (4) that the status of transient and stable states in the power network established the effectiveness of the learning algorithm in maintaining a fast convergence speed.

2. System Description

The grid-tied PV system comprises a PV array, control unit, VSI, load and transformer, and grid system. The PV system contains a model of solar SunPower SPR305E-WHT-D modules, which are connected in series and parallel to make the PV array. The PV array generation is linked to the VSI through the regulatory unit. The VSI equivalent model is available in Ammeh et al. [44], Deffaf et al. [45], and Debdouche et al. [46]. A triple-phase coupling transformer ($T1$) is employed to interface the grid and inverter sides, as shown in Figure 1. The system's operating variables are given in Table 1. The three phases grid system comprises a feeder network, step-down transformer ($T2$), synchronous generator, and resistive and inductive load. The system operates at a 60 Hz frequency, and a phase-to-ground measurement for the voltage and current is registered.

2.1. PV array

Solar cells have a nonlinear current–voltage characteristics expressed in Equation (1):

$$I = I_{ph} - I_0\left(e^{\frac{q(V+IR_s)}{nkT}} - 1\right) - \frac{V + IR_s}{R_{sh}} \tag{1}$$

where I_{ph} is the photocurrent, the diode saturation current is I_o, R_s denotes series resistance, R_{sh} represent shunt resistance, n represents the factor of diode ideality, k is the Boltzmann's constant (1.4×10^{-23}), q is the electron charge (1.6×10^{-19}), and T represents the temperature measured in kelvin.

The nonlinear relationship between current and voltage is influenced by the solar radiation and temperature. At 25 °C, the characteristics of voltage and current, as well as voltage and power plot for the solar array in the current study is shown in Figure 2. The maximum power point for the module is given in Table 2.

Figure 1
Representation of grid-tied photovoltaic system

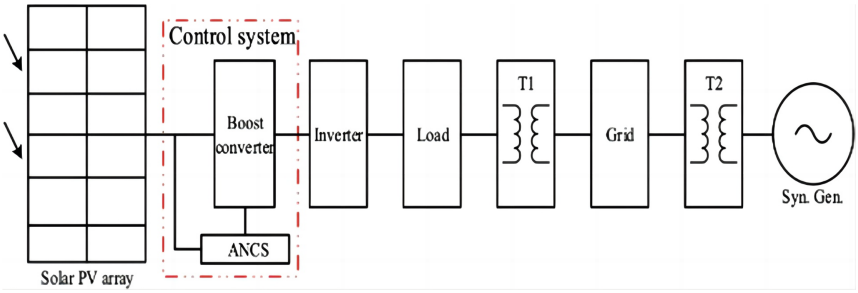

Table 1
Operating condition

Parameters	Values
Solar module power (W)	305.2
T1 power (kVA)	100
Series modules number	5
T1 primary voltage (V)	260
Parallel modules number	66
T1 secondary voltage (kV)	25
Module open-circuit voltage (V)	64.2
Module short-circuit current (A)	5.96
Capacitive load power (kVAR)	10
T2 power (MVA)	47
Resistive load power (W)	100
T2 primary voltage (kV)	120
Grid feeder length (km)	29
T2 secondary voltage (kV)	25
Syn. generator voltage (kV)	120
Feeder RL power (MW)	32
Feeder IL power (MVAR)	2
Syn. generator power (MVA)	2500

Table 2
PV array maximum power point

PV	Irradiance (kW/m^2)	Voltage (V)	Current (A)	Power (kW)
Module	0.25	53.02	1.39	0.07409
	0.5	54.17	2.78	0.15112
	1	54.70	5.58	0.30523
Array	0.25	265.10	92.23	24.45
	0.5	270.84	184.13	49.87
	1	273.50	368.28	100.72

3. Control System Design

The conventional control system design based on a mathematical model continues to provide different ways of using information from this model. This design approach sometimes neglects to account for vital information. In contrast, a data-driven control design takes cognizance of all essential information at the initial design stage. The control design of the ANCS in the current work is driven by data. However, the function of the control system is determined by the modeled neuro-fuzzy inference system, which relies on a collection of fuzzy if-then laws and a neural network machine learning model. The fuzzy identification modeling has rendered a reasonable control solution for varieties

Figure 2
Current–voltage and power–voltage characteristics under irradiance variation

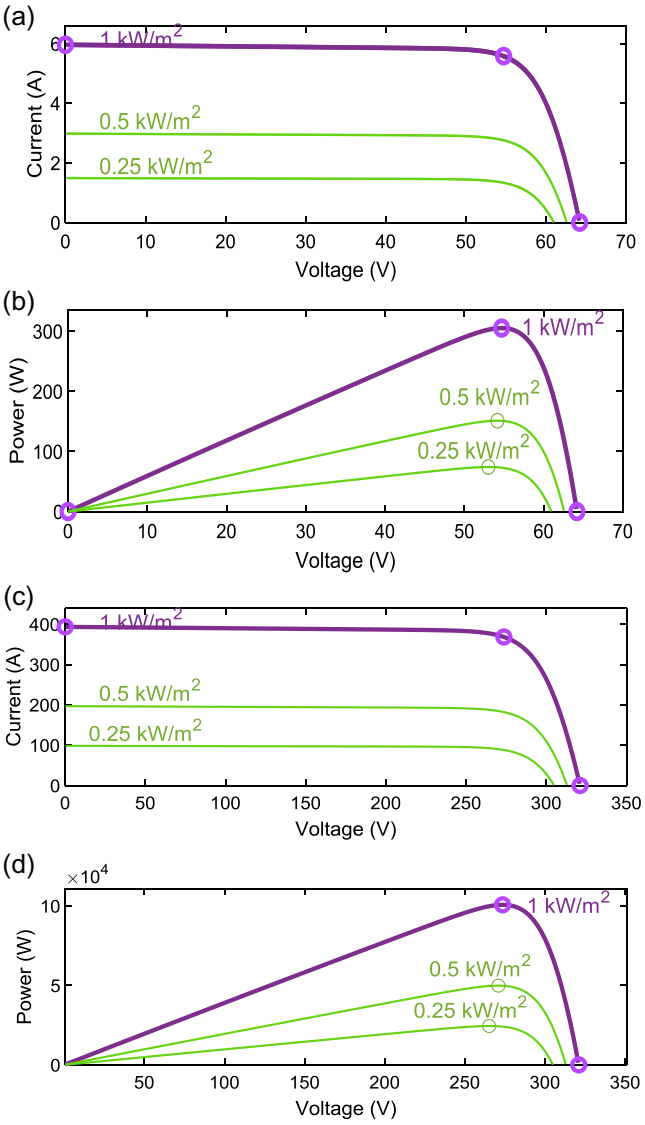

of applications since first suggested by Takagi and Sugeno [47]. In recent years, the fuzzy design approach has gained more attention in control, modeling, prediction, system identification, and monitoring applications [48–52].

The model consists of two inputs, nine rules based on Takagi and Sugeno's fuzzy if-then rules [47], and one output. Each of the inputs is associated with three membership functions which enable the partition of the input space into nine neuro-fuzzy subspaces. The if-then fuzzy-based rule regulates each subspace. The premise parameter within the rule rules defines the fuzzy subspace, while the consequence parameter determines the output portion of the fuzzy subspace. The ANCS model structure is given in Figure 3.

3.1. Sugeno–Takagi model

Sugeno fuzzy model is built within the neuro-fuzzy scheme to establish a formal framework that generated fuzzy principle from an input to output data collection. A standard fuzzy rule within a format of the Sugeno fuzzy model is as follows:

$$If\ x \text{ is } A \text{ and } y \text{ is } B \text{ THEN } z = f(x,\ y) \tag{2}$$

where A and B denote set of fuzzy in the antecedent; z is a crisp function in consequent. $f(x,\ y)$ is any functions suitable to characterize the target of the output of the scheme in the fuzzy zone as indicated by the antecedent of the laws. It is a first-order Sugeno fuzzy model when $f(x,\ y)$ is a first-order polynomial, and a zero order Sugeno fuzzy model when f is a constant. A Sugeno fuzzy model of zero order becomes functionally identical to a radial basis function network when specific minor limitations are applied.

As in Figure 3, the initial pair of the fuzzy inference operation is responsible for fuzzifying the inputs and applying the fuzzy operator. A normal rule in Sugeno fuzzy framework has the form: IF $Input\ 1 = x$ AND $Input\ 2 = y$, THEN Output is $z = ax + by + c$. For a $zero - order$ Sugeno model, the output level z is constant ($a = b = 0$). For each rule, its output level z_i is influenced by the rule's firing strength, denoted as w_i of the rule. For instance, in the case of an AND rule where Input 1 is x and Input 2 is y, the firing strength determines the weight as:

$$w_i = AndMethod(F_1(x),\ F_2(y)) \tag{3}$$

where $F_1(.),\ F_2(.)$ are functions that determine the degree of membership. Thus, the system's ultimate result is calculated by taking the weighted average of all the outputs from the rules, as presented in Equation (4). Figure 4 illustrates the example of Sugeno rule.

$$Final\ Output = \frac{\sum_{i=1}^{N} w_i z_i}{\sum_{i=1}^{N} w_i} \tag{4}$$

3.2. ANCS model

The adaptation process of the ANCS built on the learning framework of a multilayer feedforward (or backpropagation) network. The network operates in such a way that allows every individual node to execute a unique function on each node parameter and a signal entering the node. These processes grant each node to accept discrete relations in the agreement of the node parameters. The decision for the kind of node function relies on the general data exchange functions, which the adaptive system can determine. Round the adaptation process, node parameters are updated based on a specific learning procedure and assigned training data. These allow a realization of a desired input–output mapping. Consider the given adaptive network model structure in Figure 3, and assume O finite node output exists on L-layers with

Figure 3
Architecture of the model structure

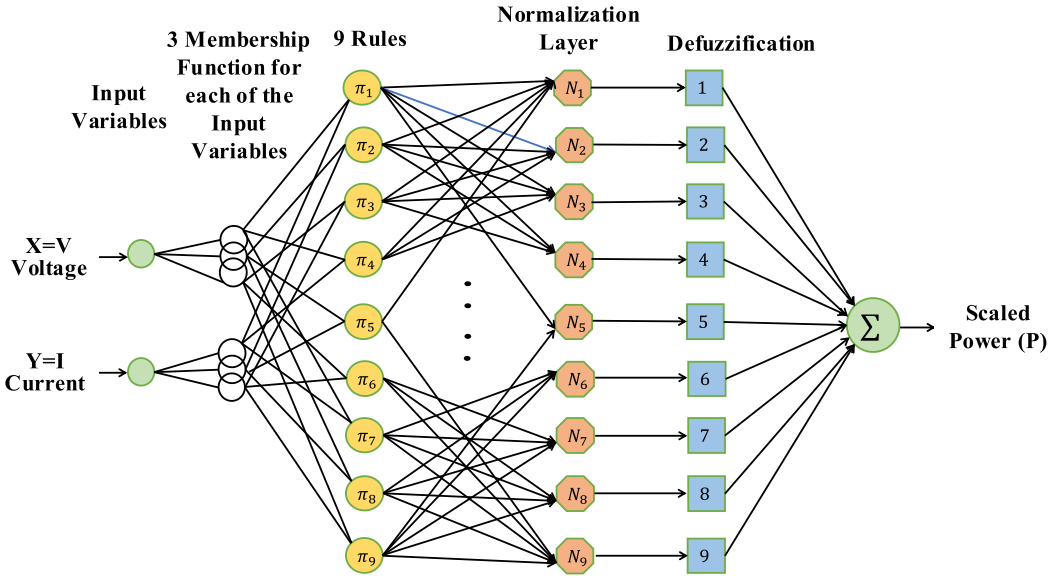

Figure 4
Illustration of Sugeno rule

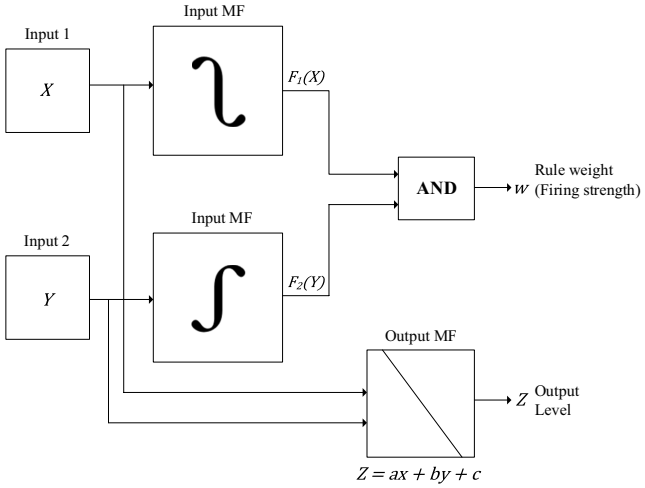

the *jth* layer corresponding to a *ith* node on that layer. If the node position on each layer makes up of *ith* then, the node output can be expressed as a function as follows:

$$O_i^j = O_i^j\left(O_1^{j-1}, \ldots O_q^{j-1}, a, b, c, \ldots\right) for\ i = 1, \ldots q \tag{5}$$

where a, b, c, and so on denote the node's parameters.

For the assigned training data, let d be the dataset instances such that the training error can be described using square errors as given below:

$$E_d = \sum_{q=1}^{R} (O_{q,d}^L - T_{q,d})^2 \tag{6}$$

where R denotes the number of layers, $T_{q,d}$ represent the qth element of the d desire outcomes vector, and $O_{q,d}^L$ denotes the qth element of the main outcomes vector generated by the d input vector.
However, the entire measured error can be evaluated as:

$$E = \sum_{d=1}^{D} E_d \tag{7}$$

To evaluate node output across the network, consider the expression of the node role for the input of the fuzzy network as follows:

$$O_i^j = \mu A_i(x) \tag{8}$$

where μ quantifies the degree of truth that error at a given time assumes linguistic value, A denotes a linguistic label associated with a node role, and x feed into the node i.
From Equation (8) with regard to layer 1:

$$\mu A_i(x) = \frac{1}{1 + \left[\left(\frac{x - C_i}{a_i}\right)^2\right]^{b_i}} \tag{9}$$

The values of the node parameters a_i, b_i, and c_i determine the configuration of the membership functions regarding linguistic label A_i.

Different types of membership functions exist, which are either piecewise differentiable or continuous functions. However, the current study adopted the Gaussian membership function. This function helps in capturing gradual transitions and gradual changes in membership degrees. The function is employed to define the shape of the adaptive neuro-fuzzy inference system's initial membership function, as shown in Figure 5. The first and second input belonging to inference system entails in Figure 5(a) and 5(b), respectively. The inference system output concerning the two input variables is shown in Figure 6(a).

However, the contribution of the neuro-fuzzy membership is computed from Equation (10):

$$f_i(x, a, c) = exp\left\{-\frac{(x - C_i)^2}{2a_i}\right\} \tag{10}$$

The parameters a and c represent the standard deviation and mean.

To ensure the appropriate value of the quantified function is determined, a combination of two Gaussian membership functions is employed to compute the adaptive neuro-fuzzy membership value. Figure 5 is determined based on the combinatory function. Figure labeled 5(a) and 5(b) represents the membership function of inputs 1 and 2, respectively, based on distinct Gaussian member functions. These functions determined the shapes of the figures.

Suppose the last number of the layer in the network shown in Figure 3 is N. The outgoing signals in the second and $(N-2)$ layers are expressed as ε and $\bar{\varepsilon}$ for each node:

$$\varepsilon_i = \mu A_i(x) \times \mu B_i(y) \text{ for } i = 1, 2, 3 \tag{11}$$

$$\bar{\varepsilon} = \frac{\varepsilon_i}{\varepsilon_1 + \varepsilon_2 + \varepsilon_3} \text{ for } i = 1, 2, 3 \tag{12}$$

From Equation (12), each node output associated with the layer determines the control strength of a rule. This strength is normalized as expressed in Equation (13) before it reaches the output layer. In the case of the node in $(N-1)$ and N-layers, the output function is given as:

$$O_i^{N-1} = \bar{\varepsilon}_i f_i \tag{13}$$

$$O_i^N = \frac{\sum_i \varepsilon_i f_i}{\sum_i \varepsilon_i} \tag{14}$$

All the membership functions for the output have a linear characteristic throughout the training process. A hybrid optimization method is adopted in identifying state parameters within the adaptive neuro-fuzzy network. The technique employed a backpropagation algorithm to tune parameters related to the input membership function within the hidden level. However, least-square estimation is adopted to identify the parameter linked to the output membership function. Figure 6(b) shows the adaptive neuro-fuzzy reasoning system, quadratic mean value error for the training and validation.

Figure 5
ANCS initial membership function

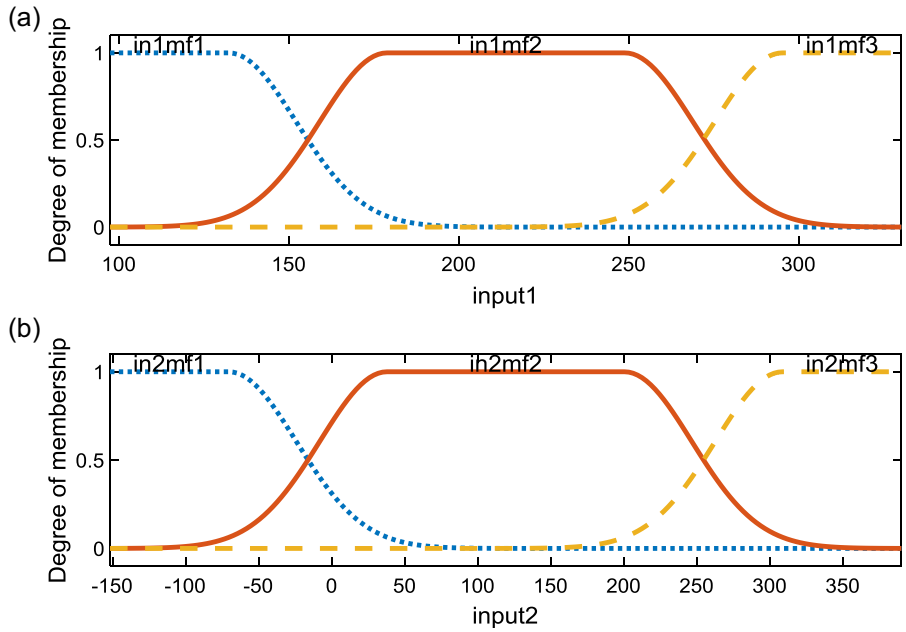

Figure 6
Adaptive neuro-fuzzy reasoning system error

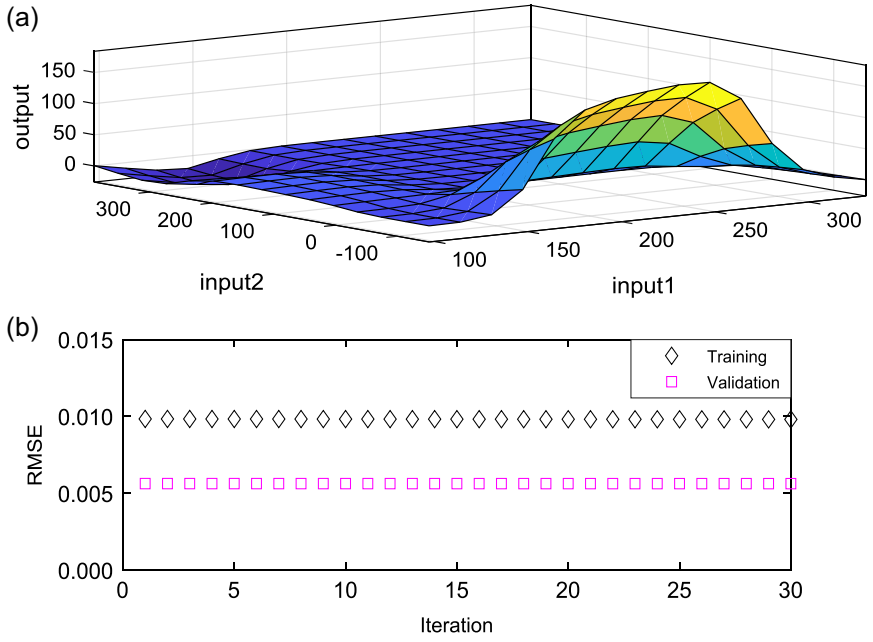

4. Simulation Results and Discussion

The examined controller operates based on diverse combinations of input–output data sources from the PV system's variables. These variables encompass solar irradiance (W/m^2), temperature ($^{\circ}C$), PV voltage (V), current (A), and power (W). These variables are taken into account because they capture the pertinent characteristics of PVs. Moreover, they can accurately depict the real performance of PV power generation. By simulation of the PV system, a wide range of values for these variables are explored, facilitating the creation of an input–output dataset. This dataset is partitioned into training and testing subsets, distributed in a ratio of 70% for training and 30% for testing. The controller's input comprises solar irradiance, temperature, voltage, and current, whereas power serves the designated output.

The current study looks at two key operating conditions that influence greatly on the PV system generation optimality. Irradiance represents the solar energy incident on the PV module.

Figure 7
Current–voltage and power–voltage characteristics under temperature variation

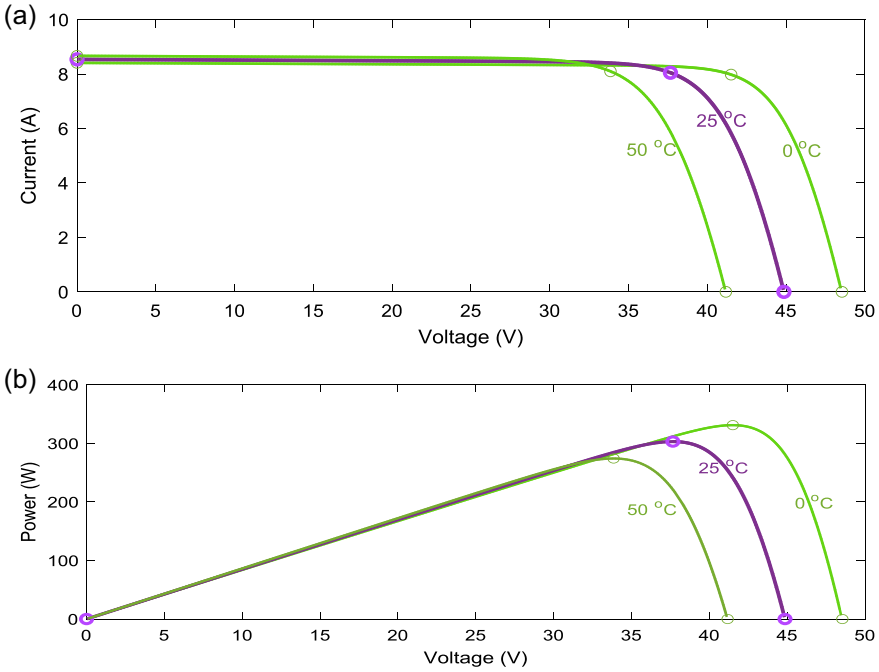

Figure 8
Off-grid power output based on MPPT controller. (a) Solar irradiance profile. (b) P&O-EADRC. (c) ANCS

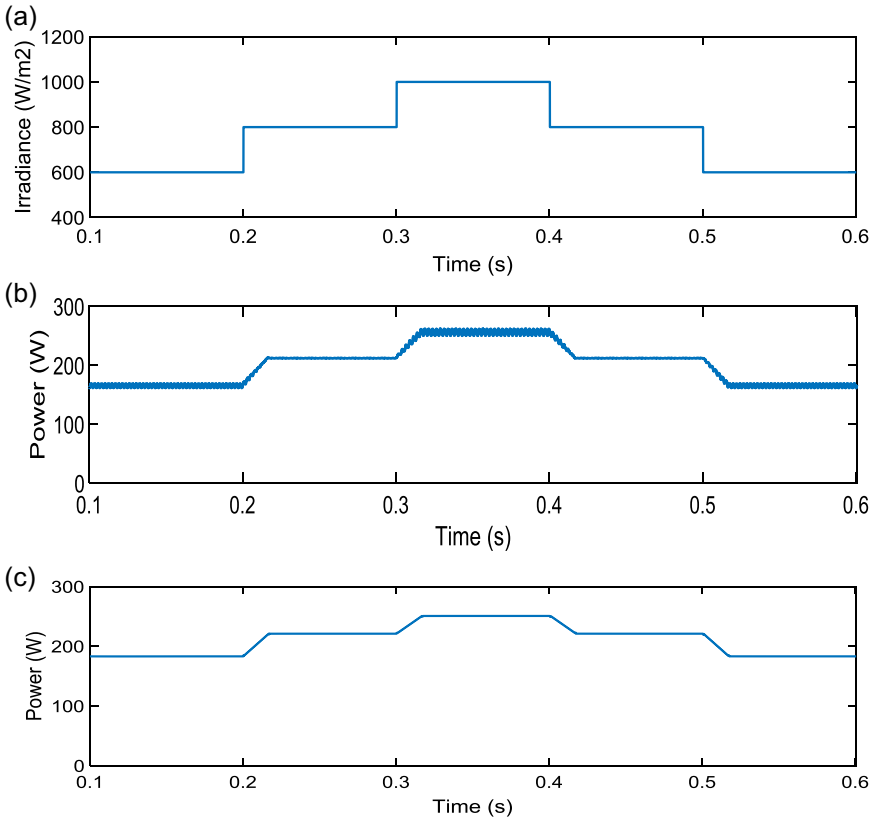

Higher irradiance levels result in increased energy absorption by the solar cells, directly influencing power output. Temperature affects the efficiency of solar cells. As temperature rises, the efficiency of PV panels tends to decrease. This decrease is a critical factor in determining the actual performance of the system under real-world conditions. These are irradiance and temperature which are capable of affecting the PV generation performance. As observed in Figure 2, the PV generation performance varies with variations in solar irradiance. The recorded single PV module power under 250 and 500 W/m^2 solar irradiance at standard test condition (STC) is 74.09 and 151.12W, respectively, as illustrated in Figure 2(b). Similarly, power generation through the PV array is 24, 450 and 49, 870W under 250 and 500 W/m^2 at STC, as shown in Figure 2(d). The effects of temperature on the PV system have remained one of the major drawbacks that challenge the PV generation performance [18, 22, 53]. Rising environmental temperature and direct sunlight striking the area surface of installed PV modules can easily trigger operating point variation in PV system energy generation. This variation is observable in Figure 7 as the PV module is subjected to temperature variation from 0 to 50 $^{\circ}$C. At 0 $^{\circ}$C, the outputted PV power is 331.25 W and decreased to 303.16 W at 25 $^{\circ}$C temperature. Similarly, the observed power at 50 $^{\circ}$C is 274.22 W while the output voltage is 33.85 V.

To carry out an assessment of the ANCS, the above two testing conditions are considered. The control system is compared with the P&O coupled with error-based active disturbance rejection control (P&O-EADRC) [54]. In the first instance, a 300 W off-grid PV system with a power generation reference of 250 W is studied and subsequently scaled up to a 100 kW grid-tied PV system. In the first case, the solar irradiance alternates from 600 W/m^2 to 800 W/m^2. The irradiance reached 1000 W/m^2 at 0.3 sec, then back to 800 W/m^2 at 0.4 sec of the runtime. Similarly, the irradiance varies from 800 to 600 W/m^2 for the remaining runtime, as shown in Figure 8(a).

The impact of the solar irradiance variation is observable in the generated power, as depicted in Figure 8(b) and (c). Both controllers exhibit effective tracking and optimizing the maximum power point. At the first half cycle of 0.2 sec, the P&O-EADRC outputs 168.36 W, and the ANCS outputs 196.59 W while there is 600 W/m^2 solar irradiance. When the irradiance increased to 1000 W/m^2, the generated power increased to 253.88 W and 254.14 W for the P&O-EADRC and ANCS, respectively. The stability of the controllers in tracking the generated power remains consistent throughout the period. However, a dither is observable while the solar irradiance is at 600 W/m^2 and 1000 W/m^2 during the P&O-EADRC operation. These suggest that the P&O-EADRC controller perturbation direction may not lead to the global MPPT.

Figure 9
Grid-tied power output based on the MPPT controller. (a) Solar irradiance profile. (b) P&O-EADRC. (c) ANCS

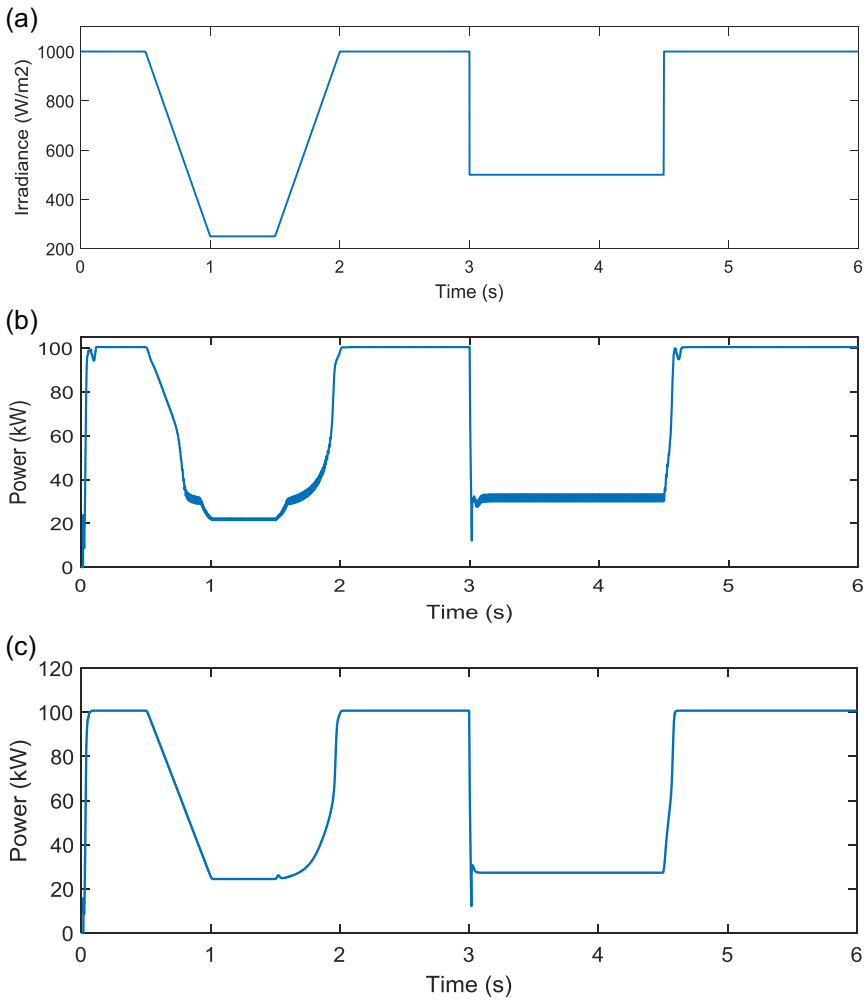

The dither then helps keep the control system from becoming stuck. The situation can lead to unwanted interaction between the dither signal and power system components.

The study's second case involves examining the controller's performance while the PV system is scaled up and connected to the grid. At the initial state, the solar irradiance is 1000 W/m^2, sharply decrease to 250 W/m^2 for 0.5 sec, and returned to its initial value during the first 3 sec. The solar irradiance suddenly reduced to 500 W/m^2 at the beginning of the remaining 3 sec and finally returned to 1000 W/m^2 after 1.5 sec, as shown in Figure 9(a). This second case considered a constant atmospheric temperature of 25 °C throughout.

The peak power point tracking occurs when the solar irradiance is at peak values, as shown in Figure 9. Also, the minimum generated power takes place while the irradiance goes to its lowest point. In the first 0.5 sec, 100.49 *kW* and 100.72 *kW* are power generated through the P&O-EADRC and ANCS, respectively. However, both MPPT-based controllers exhibit aggressive undershooting output power during the suddenly decreased solar irradiance at 3 sec. The generated power under the ANCS is free from ripples, while the generated power under the P&O-EADRC controls displayed ripple during the lowest irradiance value. These suggest the striving action of the P&O-EARDC to track the peak power output. This event validates the unwanted interaction between the controller's dither signal and sensitive power system components.

The MPPT controllers' response to the solar irradiation variation is observable in the grid-tied system current profile and voltage, displayed in Figure 10. The observed ripple in the peak generated power under the P&O-EADRC has manifested in the grid voltage and currents profile as shown in Figure 10(b) and (c). The effects of the ripples have caused an overshoot and undershoot in both grid voltage and current profile. This accounts for more than 11 A increment in the grid current under the P&O-EADRC compared with the ANCS. The observed transient response can undermine the quality of distributed power and, by extension, impact power system equipment negatively. The absence of transient voltage and current under the ANCS results from the robustness of the ANCS amid tracking the optimal power. These demonstrate the effectiveness of the soft switching capability of the control scheme adopted in the ANCS. The combined impact of both solar radiant flux and thermal state variations is observable in Figure 11. The PV system voltage demonstrates the impact of solar irradiance and thermal state. The sharp decrease in the generated power at 3 sec validates the implication of sudden solar radiance change. In contrast, the impact of sudden decrease change is severe compared to that of sudden increase change, as depicted in Figure 11(c) and (d).

A decline in power generation is observable between 2 and 3 sec while the temperature gradually increases from 25 °C to 45 °C, as shown in Figure 11(b), (c), and (d). Similarly, there is an inclined power generation while the temperature declines from 45 °C to 15 °C. The decrease in generated power in response to the increased solar temperature demonstrates the impact of temperature above the given solar PV module temperature in STCs. However, a 2.29 *kW* power increase is observable while the solar temperature decreased by 20 °C below the initial temperature. These phenomena validate the solar PV power conversion behavior concerning solar temperature [53, 55–57]. The implication in the generated power signal variation observed can lead to electromagnetic interference, affecting other electronic devices and communication systems coupled to the power grid. The variation may lead to increased losses in the distribution line due to additional heating effects. This could reduce the efficiency of distribution equipment such as transformers, circuit breakers, and other components.

Figure 10
Grid voltage and current profile. (a) Grid voltage under P&O-EADRC. (b) Enlarged grid voltage under P&O-EADRC. (c) Grid current under P&O-EADRC. (d) Grid voltage under ANCS. (e) Enlarged grid voltage under ANCS. (f) Grid current under ANCS

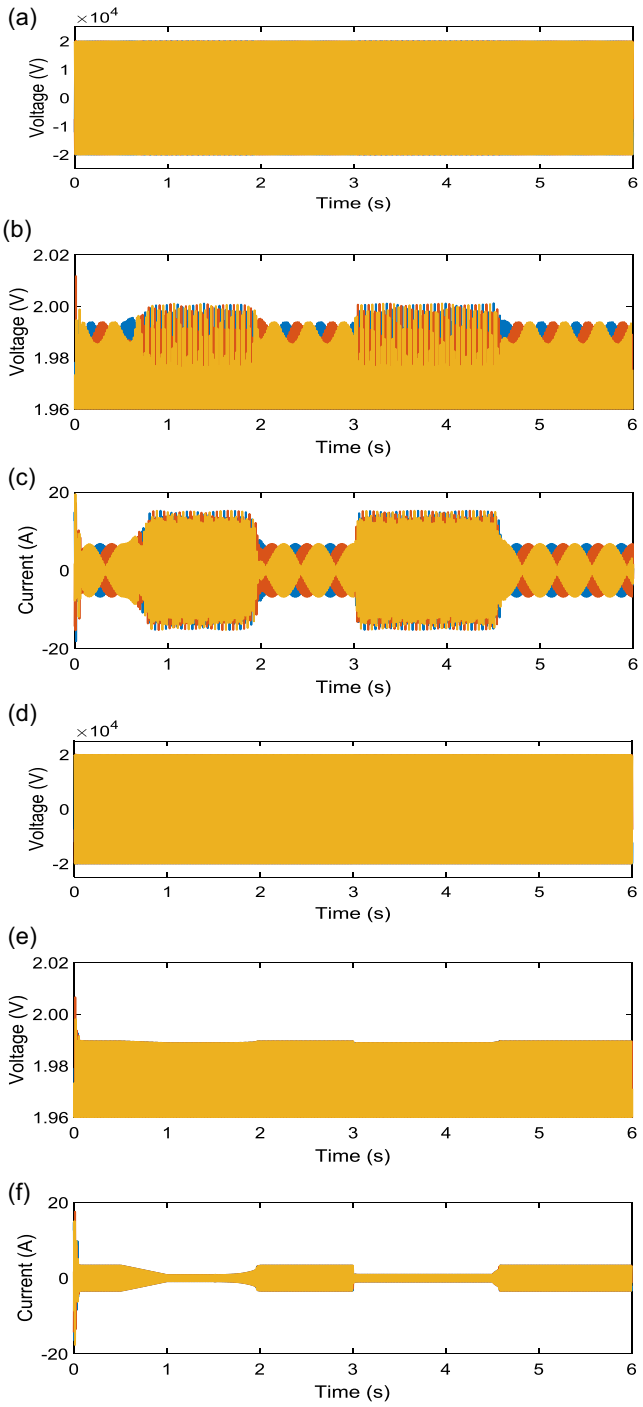

The power generation under the two controllers is consistent with the available operating condition of the PV system. However, the energy generation under the ANCS remains higher than that produced under the P&O-EADRC. As observed in

Figure 11
Grid-tied power output based on the MPPT controller. (a) Solar irradiance profile. (b) Temperature profile. (c) P&O-EADRC. (d) ANCS

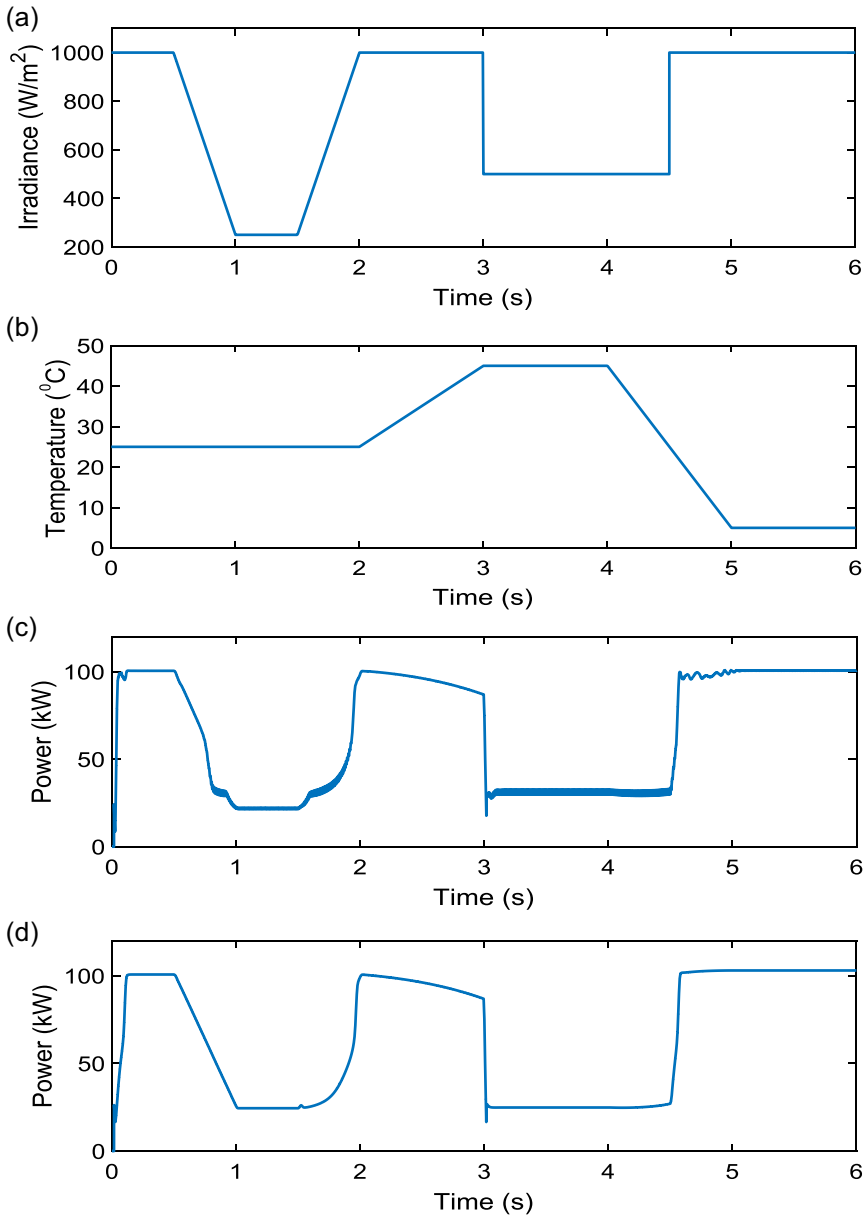

Table 3, the generated power increases with an increase in the solar irradiance, but the actual generation from the PV system lags the irradiance. These are traceable at the irradiance interval of 1000 W/m^2 at 2.99 sec and 500 W/m^2 at 3 sec, where the power generation at 2.99 sec remains until after the instantaneous change of the irradiance at 3 sec. A similar scenario is observed at 4.49 sec to 4.50 sec for the sudden solar irradiance change from 500 W/m^2 to 1000 W/m^2, respectively.

The grid voltage and current profile under the ANSC look more refined than the P&O-EADRC produced voltage profile, as observed above. The transient variation in voltage and current profiles under the P&O-EADRC appears at 1–2 sec and 3–4.5 sec intervals. However, at the initial time of the power generation, there is maximum overshoot and undershoot current. In comparison, the corresponding initial voltage spike is higher in Figure 12(a) than in Figure 12(c). These suggest the ANSC control capability in assuring stability and smooth power generation in a grid-tied PV setup.

The presence of overshoot and undershoot in the grid voltage and current profiles indicates the oscillatory behavior of the P&O-EADRC around the maximum power point. As environmental conditions change, this controller faces challenges in adapting to the new operating conditions, leading to instability. In essence, these overshoots and undershoots are indicative of the controller's dynamic behavior and its response to changing environmental conditions.

The grid voltage and current profiles under ANSC exhibit more stable behavior than P&O-EADRC. These suggest superior control capability for ensuring smoother power generation in a grid-tied PV system. The differences in dynamic behavior between the two controllers highlight the importance of controller selection for

Table 3
Power generation performance

Time (S)	Irradiance (W/m^2)	P&O-EADRC Power (kW)	ANCS Power (kW)	Temperature (°C)	P&O-EADRC Power (kW)	ANCS Power (kW)
0.5	1000	100.50	100.72	25	100.50	100.72
1.0	250	22.33	25.72	25	22.33	25.74
2.0	1000	98.51	99.25	25	98.51	99.25
3.0	500	100.49	100.64	45	86.72	86.75
4.5	1000	30.56	27.06	25	30.56	27.06
6.0	1000	100.49	100.72	5	100.70	103.01

Figure 12
Grid voltage and current profile during temperature variation. (a) Enlarged grid voltage under P&O-EADRC. (b) Grid current under P&O-EADRC. (c) Enlarged grid voltage under ANCS. (d) Grid current under ANCS

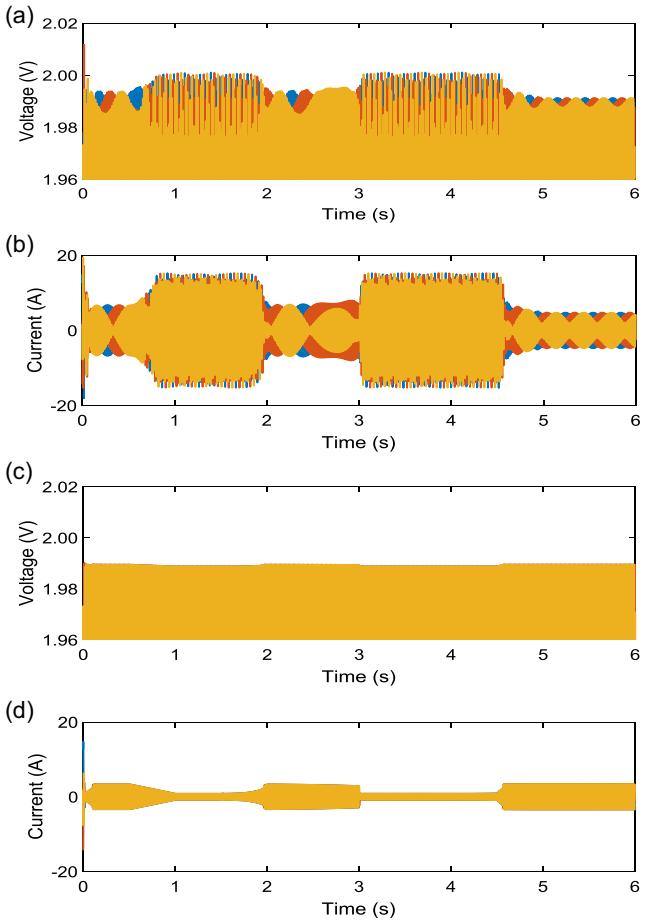

optimizing the performance of PV systems in diverse operating conditions.

5. Conclusion

The current work presented the analysis of the grid-tied PV optimal power point tracking under adaptive neuro-fuzzy control. These demonstrated the need and impact of stable power generation in a power supply network. The ANCS control outperforms the P&O-EADRC in stabilized power generation. The zero transients' voltage and current within the ANCS demonstrate the influence of the adaptive neuro-fuzzy control in enabling stable power generation. However, the impact of the irradiance and heat level on the solar grid-tied PV has been determined. However, the temperature alone contributes to a reduction of more than 15% in power generation on the grid when the temperature reached 45 °C. While the temperature drop-off to 5 °C, the generated power increases from 100.72 *kW* at 25 °C to 103.01 *kW* under ANCS. These validate the solar PV energy conversion characteristics concerning temperature.

As P&O-EADRC demonstrates transient variations in voltage and current profiles occurring at 1–2 sec and 3–4.5 sec intervals, ANSC assures stability. These imply that ANSC responds much more favorably to environmental changes, contributing to a more controlled and stable PV-tied system operation. The absence of transients under ANCS indicates a smooth transition between different operating conditions. The achieved smooth transition demonstrates stable and grid-friendly power injection. This stability is crucial for the seamless integration of grid-tied PV into the transmission network. However, the practical implications of these findings suggest that ANCS has the potential to contribute to the evolution of grid-tied PV system technology, offering insights that can guide system design, operation, and future research endeavors. Thus, this study sheds valuable light on the role of control strategies, highlighting the efficacy of ANCSs in grid-tied PV systems.

The study mainly focused on specific environmental conditions, and the generalizability of the findings to diverse climates and geographical locations warrants thorough consideration. Future research works could address these limitations by conducting extensive field studies across varied environmental contexts to validate the robustness of ANCS under diverse conditions. Exploring the scalability and adaptability of ANCS in larger-scale PV systems and its integration with emerging technologies could also be avenues for further research. Moreover, in-depth studies of the economic feasibility and cost-effectiveness of implementing ANCS in real-world applications could furnish valuable insights for industry stakeholders and policymakers.

Ethical Statement

This study does not contain any studies with human or animal subjects performed by any of the authors.

Conflicts of Interest

The authors declare that they have no conflicts of interest to this work.

Data Availability Statement

The data sharing is not applicable to this article as no new data were created or analyzed in this study.

Author Contribution Statement

Ja'afar Sulaiman Zangina: Conceptualization, Methodology, Software, Formal analysis, Investigation, Resources, Data curation, Writing – original draft, Writing – review & editing, Visualization, Supervision, Project administration. **Muhammad Aliyu Suleiman:** Methodology, Validation, Formal analysis, Investigation, Resources, Data curation, Writing – original draft, Writing – review & editing, Visualization. **Abdulla Ahmed:** Methodology, Validation, Investigation, Resources, Data curation, Writing – original draft, Writing – review & editing, Visualization.

References

[1] Behzadi, A., Thorin, E., Duwig, C., & Sadrizadeh, S. (2023). Supply-demand side management of a building energy system driven by solar and biomass in Stockholm: A smart integration with minimal cost and emission. *Energy Conversion and Management*, *292*, 117420.

[2] Hill, A. (2022). Smoothing the curve: An estimation of the cost of demand variation and the impact of solar and wind. *Resource and Energy Economics*, *70*, 101328.

[3] Li, Y., Samad, S., Ahmed, F. W., Abdulkareem, S. S., Hao, S., & Rezvani, A. (2020). Analysis and enhancement of PV efficiency with hybrid MSFLA-FLC MPPT method under different environmental conditions. *Journal of Cleaner Production*, *271*, 122195.

[4] Luo, W., Clement, C. E., Khoo, Y. S., Wang, Y., Khaing, A. M., Reindl, T., . . . , & Pravettoni, M. (2021). Photovoltaic module failures after 10 years of operation in the tropics. *Renewable Energy*, *177*, 327–335.

[5] Ma, X., Zhai, Y., Zhang, T., Yao, X., & Hong, J. (2023). What changes can solar and wind power bring to the electrification of China compared with coal electricity: From a cost-oriented life cycle impact perspective. *Energy Conversion and Management*, *289*, 117162.

[6] Neuhoff, K., May, N., & Richstein, J. C. (2022). Financing renewables in the age of falling technology costs. *Resource and Energy Economics*, *70*, 101330.

[7] Singh, R., Amrr, S. M., & Asghar, M. J. (2021). Supervisory control strategy for the effective solar energy utilization in a residential microgrid system using a cost-effective controller. *International Journal of Electrical Power & Energy Systems*, *132*, 107170.

[8] da Silveira Brito, E. M., Cupertino, A. F., Pereira, H. A., & Mendes, V. F. (2022). Reliability-based trade-off analysis of reactive power capability in PV inverters under different sizing ratio. *International Journal of Electrical Power & Energy Systems*, *136*, 107677.

[9] Mahela, O. P., & Shaik, A. G. (2017). Power quality recognition in distribution system with solar energy penetration using S-transform and fuzzy C-means clustering. *Renewable Energy*, *106*, 37–51.

[10] Mishra, M. K., & Lal, V. N. (2020). An improved methodology for reactive power management in grid integrated solar PV system with maximum power point condition. *Solar Energy*, *199*, 230–245.

[11] Patsalides, M., Efthymiou, V., Stavrou, A., & Georghiou, G. E. (2016). A generic transient PV system model for power quality studies. *Renewable Energy*, *89*, 526–542.

[12] Potter, A., Haider, R., Ferro, G., Robba, M., & Annaswamy, A. M. (2023). A reactive power market for the future grid. *Advances in Applied Energy*, *9*, 100114.

[13] Saidi, A. S. (2022). Impact of grid-tied photovoltaic systems on voltage stability of Tunisian distribution networks using dynamic reactive power control. *Ain Shams Engineering Journal*, *13*(2), 101537.

[14] Samimi, A., Kazemi, A., & Siano, P. (2015). Economic-environmental active and reactive power scheduling of modern distribution systems in presence of wind generations: A distribution market-based approach. *Energy Conversion and Management*, *106*, 495–509.

[15] Gawhade, P., & Ojha, A. (2021). Recent advances in synchronization techniques for grid-tied PV system: A review. *Energy Reports*, *7*, 6581–6599.

[16] Lezcano, H., Rodas, J., Pacher, J., Ayala, M., & Romero, C. (2023). Design and validation of a modular control platform for a voltage source inverter. *HardwareX*, *13*, e00390.

[17] Merai, M., Naouar, M. W., Slama-Belkhodja, I., & Monmasson, E. (2021). A systematic design methodology for DC-link voltage control of single phase grid-tied PV systems. *Mathematics and Computers in Simulation*, *183*, 158–170.

[18] Talha, M., Raihan, S. R. S., & Abd Rahim, N. (2020). PV inverter with decoupled active and reactive power control to mitigate grid faults. *Renewable Energy*, *162*, 877–892.

[19] Motahhir, S., El Hammoumi, A., & El Ghzizal, A. (2020). The most used MPPT algorithms: Review and the suitable low-cost embedded board for each algorithm. *Journal of Cleaner Production*, *246*, 118983.

[20] Alik, R., & Jusoh, A. (2018). An enhanced P&O checking algorithm MPPT for high tracking efficiency of partially shaded PV module. *Solar Energy*, *163*, 570–580.

[21] Devi, V. K., Premkumar, K., Bisharathu Beevi, A., & Ramaiyer, S. (2017). A modified Perturb & Observe MPPT technique to tackle steady state and rapidly varying atmospheric conditions. *Solar Energy*, *157*, 419–426.

[22] Shahid, H., Kamran, M., Mehmood, Z., Saleem, M. Y., Mudassar, M., & Haider, K. (2018). Implementation of the novel temperature controller and incremental conductance MPPT algorithm for indoor photovoltaic system. *Solar Energy*, *163*, 235–242.

[23] Doubabi, H., Salhi, I., Chennani, M., & Essounbouli, N. (2021). High Performance MPPT based on TS Fuzzy–integral backstepping control for PV system under rapid varying irradiance—Experimental validation. *ISA Transactions*, *118*, 247–259.

[24] Mohammadinodoushan, M., Abbassi, R., Jerbi, H., Ahmed, F. W., Abdalqadir Kh Ahmed, H., & Rezvani, A. (2021). A new MPPT design using variable step size perturb and observe method for PV system under partially shaded conditions by modified shuffled frog leaping algorithm-SMC controller. *Sustainable Energy Technologies and Assessments, 45*, 101056.

[25] Ali, A. I. M., & Mohamed, H. R. A. (2022). Improved P&O MPPT algorithm with efficient open-circuit voltage estimation for two-stage grid-integrated PV system under realistic solar radiation. *International Journal of Electrical Power & Energy Systems*, *137*, 107805.

[26] Ali, A. I. M., Sayed, M. A., & Mohammed, E. E. M. (2018). Modified efficient perturb and observe maximum power point tracking technique for grid-tied PV system. *International Journal of Electrical Power & Energy Systems, 99*, 192–202.

[27] Altwallbah, N. M. M., Radzi, M. A. M., Azis, N., Shafie, S., & Zainuri, M. A. A. M. (2022). New perturb and observe algorithm based on trapezoidal rule: Uniform and partial shading conditions. *Energy Conversion and Management*, *264*, 115738.

[28] Bhattacharyya, S., Kumar, P. D. S., Samanta, S., & Mishra, S. (2021). Steady output and fast tracking MPPT (SOFT-MPPT) for P&O and InC algorithms. *IEEE Transactions on Sustainable Energy*, *12*(1), 293–302.

[29] Javed, S., & Ishaque, K. (2022). A comprehensive analyses with new findings of different PSO variants for MPPT problem under partial shading. *Ain Shams Engineering Journal*, *13*(5), 101680.

[30] Refaat, A., Khalifa, A. E., Elsakka, M. M., Elhenawy, Y., Kalas, A., & Elfar, M. H. (2023). A novel metaheuristic MPPT technique based on enhanced autonomous group particle swarm optimization algorithm to track the GMPP under partial shading conditions – Experimental validation. *Energy Conversion and Management*, *287*, 117124.

[31] Yang, B., Wu, S., Huang, J., Guo, Z., Wang, J., Zhang, Z., . . . , & Jiang, L. (2023). Salp swarm optimization algorithm based MPPT design for PV-TEG hybrid system under partial shading conditions. *Energy Conversion and Management*, *292*, 117410.

[32] Bouakkaz, M. S., Boukadoum, A., Boudebbouz, O., Bouraiou, A., Boutasseta, N., & Attoui, I. (2020). ANN based MPPT algorithm design using real operating climatic condition. In *2020 2nd International Conference on Mathematics and Information Technology*, 159–163.

[33] de Dieu Nguimfack-Ndongmo, J., Ngoussandou, B. P., Goron, D., Asoh, D. A., Kidmo, D. K., Nfah, E. M., & Kenné, G. (2022). Nonlinear neuro-adaptive MPPT controller and voltage stabilization of PV systems under real environmental conditions. *Energy Reports*, *8*, 1037–1052.

[34] Hussein, I., Çelik, Ö., & Teke, A. (2022). A hybrid random parameters modification to MPPT algorithm to mitigate interharmonics from single-phase grid-connected PV systems. *Energy Reports*, *8*, 6234–6244.

[35] Issaadi, S., Issaadi, W., & Khireddine, A. (2019). New intelligent control strategy by robust neural network algorithm for real-time detection of an optimized maximum power tracking control in photovoltaic systems. *Energy*, *187*, 115881.

[36] Mohamed, A. A., Metwally, H., El-Sayed, A., & Selem, S. I. (2019). Predictive neural network based adaptive controller for grid-connected PV systems supplying pulse-load. *Solar Energy*, *193*, 139–147.

[37] Verma, P., Garg, R., & Mahajan, P. (2020). Asymmetric interval type-2 fuzzy logic control based MPPT tuning for PV system under partial shading condition. *ISA Transactions, 100*, 251–263.

[38] Yang, B., Yu, T., Shu, H., Zhu, D., An, N., Sang, Y., & Jiang, L. (2018). Energy reshaping based passive fractional-order PID control design and implementation of a grid-connected PV inverter for MPPT using grouped grey wolf optimizer. *Solar Energy*, *170*, 31–46.

[39] Kandemir, E., Cetin, N. S., & Borekci, S. (2017). A comprehensive overview of maximum power extraction methods for PV systems. *Renewable and Sustainable Energy Reviews, 78*, 93–112.

[40] Munteanu, I., & Bratcu, A. I. (2015). MPPT for grid-connected photovoltaic systems using ripple-based extremum seeking control: Analysis and control design issues. *Solar Energy*, *111*, 30–42.

[41] Neçaibia, A., Ladaci, S., Charef, A., & Loiseau, J. J. (2015). Fractional order extremum seeking approach for maximum power point tracking of photovoltaic panels. *Frontiers in Energy, 9*, 43–53.

[42] Silveira, R. D., das Neves, G. P., da Silva, S. A. O., & Angélico, B. A. (2021). An enhanced MPPT algorithm based on adaptive extremum-seeking control applied to photovoltaic systems operating under partial shading. *IET Renewable Power Generation*, *15*(6), 1227–1239.

[43] Joisher, M., Singh, D., Taheri, S., Espinoza-Trejo, D. R., Pouresmaeil, E., & Taheri, H. (2020). A hybrid evolutionary-based MPPT for photovoltaic systems under partial shading conditions. *IEEE Access*, *8*, 38481–38492.

[44] Ammeh, L., El Fadil, H., Oulcaid, M., Giri, F., & Ahmed-Ali, T. (2020). Adaptive output feedback controller of voltage source inverters in microgrid connected mode. *IFAC PapersOnLine*, *53*(2), 12876–12881.

[45] Deffaf, B., Farid, H., Benbouhenni, H., Medjmadj, S., & Debdouche, N. (2023). Synergetic control for three-level voltage source inverter-based shunt active power filter to improve power quality. *Energy Reports*, *10*, 1013–1027.

[46] Debdouche, N., Zarour, L., Benbouhenni, H., Mehazzem, F., & Deffaf, B. (2023). Robust integral backstepping control microgrid connected photovoltaic system with battery energy storage through multi-functional voltage source inverter using direct power control SVM strategies. *Energy Reports*, *10*, 565–580.

[47] Takagi, T., & Sugeno, M. (1985). Fuzzy identification of systems and its applications to modeling and control. *IEEE Transactions on Systems, Man, and Cybernetics*, *SMC-15*(1), 116–132.

[48] Bilal, B., Adjallah, K. H., Sava, A., Yetilmezsoy, K., & Kıyan, E. (2022). Wind power conversion model identification using adaptive neuro-fuzzy inference systems: A case study. *Energy*, *239*, 122089.

[49] Côrtes, H. M., Santos, P. E., & da Silva Filho, J. I. (2022). Monitoring electrical systems data-network equipment by means of fuzzy and paraconsistent annotated logic. *Expert Systems with Applications*, *187*, 115865.

[50] Du, S., Wu, M., Chen, L., & Pedrycz, W. (2021). Prediction model of burn-through point with fuzzy time series for iron ore sintering process. *Engineering Applications of Artificial Intelligence*, *102*, 104259.

[51] Škrjanc, I. (2021). An evolving concept in the identification of an interval fuzzy model of Wiener-Hammerstein nonlinear dynamic systems. *Information Sciences*, *581*, 73–87.

[52] Wang, Y., Yang, M. H., Zhang, H. Y., Wu, X., & Hu, W. X. (2022). Data-driven prediction method for characteristics of voltage sag based on fuzzy time series. *International Journal of Electrical Power & Energy Systems, 134*, 107394.

[53] Gong, Y., Wang, Z., Lai, Z., & Jiang, M. (2021). TVACPSO-assisted analysis of the effects of temperature and irradiance on the PV module performances. *Energy*, *227*, 120390.

[54] Hou, G., Ke, Y., & Huang, C. (2021). A flexible constant power generation scheme for photovoltaic system by error-based active disturbance rejection control and perturb & observe. *Energy*, *237*, 121646.

[55] Aboagye, B., Gyamfi, S., Ofosu, E. A., & Djordjevic, S. (2021). Degradation analysis of installed solar photovoltaic (PV) modules under outdoor conditions in Ghana. *Energy Reports*, *7*, 6921–6931.

[56] Toledo, C., López-Vicente, R., Abad, J., & Urbina, A. (2020). Thermal performance of PV modules as building elements: Analysis under real operating conditions of different technologies. *Energy and Buildings*, *223*, 110087.

[57] Zhao, Y., Gong, S., Zhang, C., Ge, M., & Xie, L. (2022). Performance analysis of a solar photovoltaic power generation system with spray cooling. *Case Studies in Thermal Engineering*, *29*, 101723.

How to Cite: Zangina, J. S., Suleiman, M. A., & Ahmed, A. (2025). Analysis of Grid-Tied Solar Photovoltaic Energy Generation Under Uncertain Atmospheric Conditions Using Adaptive Neuro-Fuzzy Control System. *Archives of Advanced Engineering Science*, *3*(2), 111–123. https://doi.org/10.47852/bonviewAAES42022110